Spin-Orbit *Ab Initio* Investigation of the Photodissociation of Dibromomethane in the Gas and Solution Phases

YAJUN LIU,[1] HONGYAN XIAO,[1] MENGTAO SUN,[2] WEIHAI FANG[1]
[1]*College of Chemistry, Beijing Normal University, Beijing 100875, People's Republic of China*
[2]*Beijing National Laboratory for Condensed Matter Physics, Institute of Physics, Chinese Academy of Sciences, Beijing 100080, People's Republic of China*

Received 11 September 2007; Revised 12 March 2008; Accepted 14 March 2008
DOI 10.1002/jcc.21008
Published online 12 May 2008 in Wiley InterScience (www.interscience.wiley.com).

Abstract: A clear and reliable theoretical investigation on dibromomethane (CH_2Br_2) photodissociation is desired. The calculation must consider: (i) relativistic effects; (ii) the potential energy curves (PECs) of spin-orbit coupling states; (iii) geometry optimization by the method with both static and dynamic electron correlations; (iv) solvent effects on the photodissociation in the solution. All these have been considered in this study by state-of-the-art quantum chemical calculations. The experimentally observed photodissociation in the gas phase with products of spin-orbit-coupled states, $Br(^2P_{3/2})$ and $Br^*(^2P_{1/2})$, was assigned by multi-state second order multiconfigurational perturbation theory in conjunction with spin-orbit interaction through complete active space state interaction (MS-CASPT2/CASSI-SO) PECs. The mechanisms of the experimentally observed photodissociation and photoisomerization in solvent were elucidated by the MS-CASPT2/CASSI-SO method combined with polarized continuum model of the solvent.

 J Comput Chem 29: 2513–2519, 2008

Key words: photodissociation; potential energy curve; spin-orbit coupling; solvent effect; MS-CASPT2

Introduction

The interest in the study of the photodissociations of polyhalomethane molecules has increased considerably in the last years. Molecules such as CH_2XY (X, Y = Cl, Br, and I) have been observed in the troposphere, and consequently considered as important sources of reactive halogens in the atmosphere.[1–4] CH_2Br_2 and CH_2I_2 have been widely used as reagents for cyclopropanation reactions with alkenes.[5–8] From a fundamental viewpoint, photodissociation studies involving polyhalomethanes are helpful for exploring fundamental photochemical reaction mechanisms. For CH_2Br_2, there are rich experimental literatures on its ultraviolet absorption and photoelectron spectra,[9–12] thermochemical data of photofragmentations,[13–16] and photodissociation dynamics.[17–22] The photodissociation of CH_2Br_2 has been investigated by all kinds of experimental techniques from different angles. Phillips and coworkers.[17] obtained A-band resonance Raman spectra of CH_2Br_2 in the gas and solution phases and nanosecond time-resolved resonance Raman spectra of CH_2Br_2 photoproducts. Lee et al.[19] determined a simple C—Br bond fission of CH_2Br_2 at 248 nm by using product translational spectroscopy. Zhang and coworkers[21] investigated the photodissociation dynamics of CH_2Br_2 and measured the branching ratios of $Br^*(^2P_{1/2})/Br(^2P_{3/2})$ at 234 and 267 nm. Wei et al.[22] observed Br_2 molecular elimination in 248 nm photolysis of CH_2Br_2 by using cavity ring-down absorption spectroscopy. One common conclusion of those experiments is that a simple C—Br bond cleavage is a main fast photodissociation channel of CH_2Br_2 in both gas and solution phases. In addition, CH_2Br_2 may turn a photodissociation into a photoisomerization in the solution phase.

Although there are rich experimental investigations, the detailed photodissociation process and mechanism of CH_2Br_2 are still not clear. It is in dire need of a clear reliable theoretical calculation in both gas and solution phases. The reliable calculation must consider: (i) relativistic effects since bromine is a heavy atom; (ii) the PECs of spin-orbit coupling states, which are very necessary to clearly describe the photodissociation channels leading to the products $Br(^2P_{3/2})$ and $Br^*(^2P_{1/2})$; (iii) geometry optimization by the method with both static and dynamic electron correlations, since the complete active space

Additional Supporting Information may be found in the online version of this article.

Correspondence to: Y. Liu; e-mail: yajun.liu@bnu.edu.cn

Contract/grant sponsor: National Natural Science Foundation of China; contract/grant numbers: 20673012, 20720102038, 20573011, 10625418, 20703064

Contract/grant sponsor: Major State Basic Research Development Programs; contract/grant numbers: 2004CB719903, 2007CB815206

Table 1. The Geometries of CH_2Br_2, CH_2Br-Br and the TS Between them (Bond Lengths in Å and Bond Angles in Degrees).

Species	State	Method	R(C−H)	R(C−Br)	R(Br−Br)	∠HCH	∠HCBr	∠BrCBr	∠CBrBr
CH_2Br_2	S_0	CASPT2	1.091	1.925		112.2	108.0	112.9	
		CASPT2 + PCM	1.092	1.927		112.4	108.0	112.7	
		QCISD[a]	1.086	1.945		111.6		114.2	
		Exp.	1.097,[b] 1.085[c]	1.925,[b] 1.933[c]		110.9,[b] 112.4[c]		112.9,[b] 112.6[c]	
	S_1	CASPT2	1.094	2.257		119.9	112.8	78.3	
		CASPT2 + PCM	1.095	2.265		120.2	112.8	77.9	
	S_2	CASPT2	1.093	2.229		116.5	98.1	149.0	
	T_1	CASPT2	1.094	2.213		117.8	112.9	82.3	
	T_2	CASPT2	1.096	2.182		112.8	99.7	144.4	
CH_2Br-Br	S_0	CASPT2	1.084	1.786	2.634	121.3	117.3	36.1	120.3
		CASPT2 + PCM	1.084	1.783	2.649	121.6	117.5	36.4	120.0
		B3LYP[d]	1.078	1.768	2.674		118.1		122.0
		MP2[e]	1.082	1.785	2.782	121.7	117.4		118.3
	S_1	CASPT2	1.081	1.853	4.232	123.6	117.4	84.2	70.0
		CASPT2 + PCM	1.082	1.855	4.250	123.9	117.2	84.7	69.6
TS	S_0	CASPT2	1.082	1.785, 3.013	2.898	123.6	99.0, 118.2	68.9	76.0, 35.1

[a]Ref. 34.
[b,c]Results based on microwave studies in Refs. 32 and 33.
[d]Ref. 17.
[e]Ref. 35.

self-consistent field (CASSCF) optimization on the weak C—Br bond could produce a very big deviation in the equilibrium geometry[23]; (iv) solvent effects on the photodissociation in the solution. In the current theoretical investigation on the photochemistry of CH_2Br_2, we considered all the above aspects.

Methodology and Computational Details

The geometrical optimizations and vibrational frequency analyses were performed by using the complete active space second order perturbation (CASPT2)[24] method. The multi-state CASPT2 (MS-CASPT2)[25] was used to calculate the T_v values and oscillator strengths (f) of the spin-free states. The T_v and f values of the spin-coupled states were evaluated by the MS-CASPT2/CASSI-SO approach[26] in conjunction with atomic mean-field integral (AMFI) approximation.[27] The so-called IPEA-shift with a value of 0.25 was used in all the (MS-)CASPT2 calculations.[28] The C [He] and Br [Ar] cores were not correlated at the MS-CASPT2 level. The experimentally employed solvent cyclohexane was modeled via polarized continuum model (PCM).[29] The selected active space comprises 12 electrons in 10 orbitals for CH_2Br_2 and CH_2Br-Br. The relativistic basis sets of the atomic natural orbital type, ANO-RCC,[30] were used for all the above calculations. For the geometry optimizations, frequency analyses, and calculations of PECs, the H, C and Br bases were contracted to 2s1p, 3s2p1d, and 5s4p2d1f, respectively. For the calculations of the T_v and f values at equilibrium structures, a larger contraction of 3s2p1d for H, 4s3p2d1f for C and 6s5p3d2f1g for Br was used. All the calculations were performed using the MOLCAS 6.4 quantum chemistry software.[31]

Results and Discussion

Geometries of CH_2Br_2 and CH_2Br-Br

The first three singlet and first two triplet states of CH_2Br_2, and the first two singlet states of CH_2Br-Br were located by the CASPT2 optimizations. The presently located geometries were compared with the previously optimized and available experimental ones in Table 1. For the schematic molecular structures, see Figure 1. The CASPT2 optimized bond length R(C—Br) and bond angle ∠BrCBr of the CH_2Br_2 ground state (1^1A_1) are nearly the same as the experimentally detected ones,[32,33] respectively. The CASPT2 calculated harmonic vibrational frequencies of the CH_2Br_2 and CH_2Br-Br ground states were listed in Tables 2 and 3, respectively. The present results were compared with the previous QCISD[34] and DFT[17] calculated and experimental values.[35–37] As shown in Tables 2 and 3, the CASPT2 calculated vibrational frequencies were well or reasonably consistent with the corresponding experimental values.

We also optimized the geometries of the ground and first singlet excited states of CH_2Br_2 and CH_2Br-Br in cyclohexane solvent by the CASPT2 + PCM method. By the comparison in Table 1, the solvent has little effect on the geometries of CH_2Br_2. However, it does affect the weak Br—Br bond of CH_2Br-Br, which is elongated 0.015 and 0.018 Å in the solution for the $1^1A'$ and $1^1A''$ states, respectively. The harmonic vibrational frequencies of CH_2Br_2 and CH_2Br-Br ground states were also computed by the CASPT2 + PCM method. As shown in Tables 2 and 3, the calculated results of vibrational frequencies by considering solvent effects are in better agreement with the experimentally observed values.

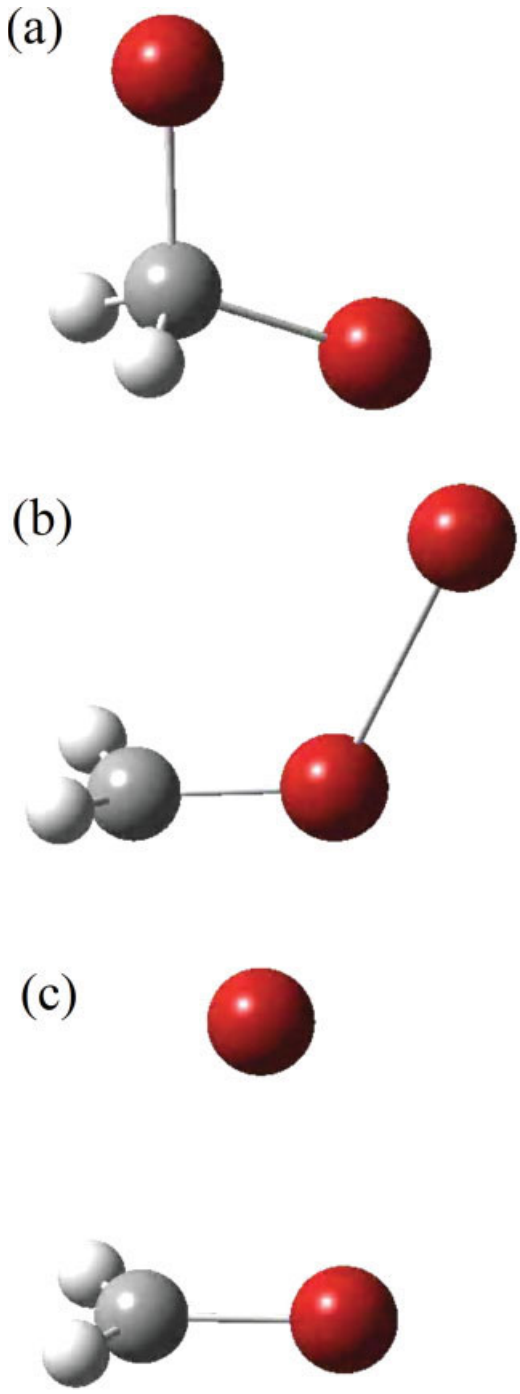

Figure 1. Schematic diagrams depicting the CASPT2 equilibrium geometries of (a) 1^1A_1, 1^1B_1, 1^1B_2, 1^3B_1, and 1^3B_2 of CH_2Br_2; (b) $1^1A'$ of $CH_2Br—Br$; (c) $1^1A''$of $CH_2Br—Br$, this structure is similar to that of the TS between CH_2Br_2 and $CH_2Br—Br$.

Vertical Excitation Energies of CH_2Br_2

In 1975, Causley et al.[9] observed the diffuse absorption bands in UV spectrum (denoted as A-bands) of CH_2Br_2 and assigned two band maxima 45,590 cm^{-1} (5.65 eV) and 51,490 cm^{-1} (6.38 eV) relevant to $n(b_1 + b_2) \rightarrow \sigma^*$ and $n(a_1 + a_2) \rightarrow \sigma^*$ transitions, respectively. Their experimental f values are 0.024 and 0.014,[9] respectively. The T_v and f values of the first six singlet and the first six triplet excited states of CH_2Br_2 were calculated by the MS-CASPT2//CASPT2 method. The calculated results were compared with the previous TD-B3LYP[21b] and MRDCI[22] calculated ones in Table 4. Those very high states have nothing to do with our concerns and were not tabulated. The T_v (f) values of the first four singlet and the first four triplet excited states of CH_2Br_2 in cyclohexane were also calculated with consideration of solvent effects by the MS-CASPT2 + PCM//CASPT2 + PCM method (cf. Table 4). Compared with the results in the gas phase, the T_v values have not obvious changes in the solution phase. It is evidence that the solvent has little effect on the T_v values of CH_2Br_2.

The T_v (f) values of seventeen spin-coupled states composed of the first five singlet and four triplet spin-free states in Table 4 were evaluated by the MS-CASPT2/CASSI-SO//CASPT2 and MS-CASPT2 + PCM/CASSI-SO//CASPT2 + PCM methods.

Table 2. The Calculated CH_2Br_2 Harmonic Vibrational Frequencies in Comparison with the Experimental Values (in cm^{-1}).

Vibrational mode	CASPT2	CASPT2 + PCM	QCISD[a]	Exp.[b]	Exp.[c]
CH sym. stretch	3118	3128	3020	3009	
CH_2 bend	1438	1434	1400	1382	1388 (1388)
CBr sym. stretch	589	569	562	588	587 (576)
CBr_2 bend	152	173	167	169	179 (174)
CH asym. stretch	3206	3230	3094	3073	
CH_2 rock	821	822	791	812	
CH_2 wag	1326	1227	1206	1195	
CBr asym. stretch	596	648	646	653	640 (637)
CH_2 twist	1121	1125	1094	1095	

[a]Scaled by 0.955.[34]
[b]Ref. 36.
[c]Frequencies observed in the gas phase and the ones in the parentheses observed in cyclohexane solution.[17]

Table 3. The Calculated $CH_2Br—Br$ Harmonic Vibrational Frequencies in Comparison with the Experimental Values (in cm^{-1}).

Vibrational mode	CASPT2	CASPT2 + PCM	B3LYP[a]	Exp.[a]	Exp.[b]
CH sym. stretch	3203	3204	3152		3030
CH_2 bend	1438	1409	1428		1334
CBr stretch	824	825	858		
CH_2 wag	670	697	738	690	684, 695
Br—Br stretch	193	190	180	176	
C—Br—Br bend	138	129	133	146	
CH asym. stretch	3358	3356	3286		3156
CH_2 rock	972	957	966	960	
CH_2 twist	446	430	468	480	

[a]Ref. 17.
[b]From infrared absorption spectra in low-temperature matrixes in Refs. 35 and 37.

Table 4. The Calculated T_v (in eV) and f (in parentheses). Values of the First Four Singlet and the First Four Triplet Excited States of CH_2Br_2.

State	MS-CASPT2// CASPT2	MS-CASPT2 + PCM// CASPT2 + PCM	TD-UB3LYP// UB3LYP[a]	MRDCI// B3LYP[b]
1^1A_1	0.00	0.00	0.00	0.00
1^1B_1	5.64 (2.69 E − 02)	5.63 (2.78 E − 02)	5.34 (0.0001)	5.94
1^1B_2	5.80 (6.98 E − 03)	5.81 (6.67 E − 03)	5.36 (0.0290)	5.96
1^1A_2	5.99 (0.00 E + 00)	5.98 (0.00 E + 00)	5.69 (0.0000)	
2^1A_1	6.29 (2.45 E − 04)	6.28 (1.25 E − 04)	5.90 (0.0013)	
1^3B_1	5.19	5.19	4.81	5.32
1^3B_2	5.26	5.25	4.94	5.48
1^3A_2	5.50	5.49	5.21	
1^3A_1	5.71	5.74	5.34	

[a]Ref. 21b.
[b]Ref. 22.

The calculated T_v and f values and the compositions of the spin-free states in each spin-coupled state were listed in Table 5. According to the T_v and f values and the transition properties, we assign the experimentally[9] observed two band maxima 45,590 and 51,490 cm^{-1} to $4B_1$ and $5A_1$ states, respectively.

Vertical Excitation Energies of $CH_2Br—Br$

We calculated the T_v (f) values of the first six singlet and the first six triplet excited states of $CH_2Br—Br$ by the MS-CASPT2//CASPT2 method. The values of the first three singlet and the first three triplet excited states were listed in Table 6 and compared with the previous URPA calculated results.[17] We also calculated the T_v (f) values of the first three singlet and the first three triplet excited states of $CH_2Br—Br$ in cyclohexane by the MS-CASPT2 + PCM//CASPT2 + PCM method, see Table 6. Compared with the results in the gas phase, the T_v values have a decrease tendency in the solution phase.

The T_v (f) values of thirteen spin-coupled states composed of the first four singlet and three triplet spin-free states in Table 6 were evaluated by the MS-CASPT2/CASSI-SO//CASPT2 and MS-CASPT2 + PCM/CASSI-SO//CASPT2 + PCM methods. Table 7 listed the calculated T_v and f values and the compositions of the spin-free states in each spin-coupled state. As shown

Table 5. The Calculated T_v (in eV) and f (in parentheses) Values and Characteristics of the Low-Lying Spin-Coupled States of CH_2Br_2 in the Gas and Solution Phases.

	MS-CASPT2/CASSI-SO//CASPT2		MS-CASPT2 + PCM/CASSI-SO//CASPT2 + PCM	
State	$T_v(f)$	Characteristic	$T_v(f)$	Characteristic
$1A_1$	0.00	99.9% 1^1A_1	0.00	99.9% 1^1A_1
$1B_2$	5.24 (2.60 E − 06)	91.2% 1^3B_1, 6.8% 1^3B_2, 1.9% 1^3A_2	5.23 (3.29 E − 06)	91.8% 1^3B_1, 6.4% 1^3B_2, 1.8% 1^3A_2
$1A_2$	5.24 (0.00 E + 00)	92.8% 1^3B_1, 6.4% 1^3B_2	5.24 (0.00 E + 00)	93.4% 1^3B_1, 5.8% 1^3B_2
$2A_1$	5.24 (4.19 E − 05)	96.0% 1^3B_1, 2.2% 1^3A_2	5.24 (3.89 E − 05)	96.1% 1^3B_1, 2.0% 1^3A_2
$1B_1$	5.47 (7.46 E − 04)	92.5% 1^3B_2, 6.0% 1^3A_1, 1.5% 1^1B_1	5.48 (7.61 E − 04)	92.0% 1^3B_2, 6.4% 1^3A_1, 1.5% 1^1B_1
$2A_2$	5.49 (0.00 E + 00)	85.8% 1^3B_2, 9.4% 1^3A_1, 4.8% 1^3B_1	5.49 (0.00 E + 00)	85.6% 1^3B_2, 10.0% 1^3A_1, 4.2% 1^3B_1
$3A_1$	5.51 (5.85 E − 07)	91.0% 1^3B_2, 5.8% 1^3B_1, 1.7% 1^3A_2	5.51 (1.12 E − 06)	91.2% 1^3B_2, 5.2% 1^3B_1, 1.7% 1^3A_2, 1.8% 2^1A_1
$2B_1$	5.65 (1.92 E − 03)	84.6% 1^3A_2, 9.6% 1^1B_1, 5.8% 1^3A_1	5.66 (2.12 E − 03)	83.6% 1^3A_2, 9.8% 1^1B_1, 6.4% 1^3A_1
$4A_1$	5.68 (4.30 E − 05)	92.8% 1^3A_2, 3.8% 1^3A_1, 2.4% 1^3B_1	5.69 (4.62 E − 05)	92.0% 1^3A_2, 4.6% 1^3A_1, 2.3% 1^3B_1
$2B_2$	5.69 (1.30 E − 05)	96.0% 1^3A_2, 2.8% 1^3B_1, 1.0% 1^3B_2	5.70 (1.41 E − 05)	96.1% 1^3A_2, 2.6% 1^3B_1, 1.0% 1^3B_2
$3B_2$	5.77 (8.28 E − 04)	80.0% 1^3A_1, 15.1% 1^1B_2, 4.6% 1^3A_2	5.77 (7.18 E − 04)	80.2% 1^3A_1, 13.8% 1^1B_2, 5.8% 1^3A_2
$3B_1$	5.82 (5.36 E − 03)	74.2% 1^3A_1, 11.6% 1^3A_2, 11.0% 1^1B_1, 3.2% 1^3B_2	5.81 (5.11 E − 03)	74.2% 1^3A_1, 12.4% 1^3A_2, 9.8% 1^1B_1, 3.6% 1^3B_2
$3A_2$	5.83 (0.00 E + 00)	89.7% 1^3A_1, 7.8% 1^3B_2, 2.0% 1^3B_1	5.83 (0.00 E + 00)	89.1% 1^3A_1, 8.4% 1^3B_2, 2.0% 1^3B_1
$4B_1$	5.94 (2.04 E − 02)	77.5% 1^1B_1, 14.0% 1^3A_1, 4.3% 1^3B_2, 3.6% 1^3A_2	5.94 (2.17 E − 02)	78.4% 1^1B_1, 12.8% 1^3A_1, 4.3% 1^3B_2, 3.8% 1^3A_2
$4B_2$	6.02 (4.73 E − 03)	83.0% 1^1B_2, 15.0% 1^3A_1, 1.5% 1^3B_1	6.03 (4.58 E − 03)	84.3% 1^1B_2, 13.8% 1^3A_1, 1.4% 1^3B_1
$4A_2$	6.23 (0.00 E + 00)	98.9% 1^1A_2	6.24 (0.00 E + 00)	98.8% 1^1A_2
$5A_1$	6.36 (6.80 E − 03)	98.1% 2^1A_1	6.27 (4.10 E − 03)	97.7% 2^1A_1, 1.4% 1^1B_2

Table 6. The Calculated T_v (in eV) and f (in parentheses) Values of the First Three Singlet and the First Three Triplet Excited States of CH_2Br-Br.

State	MS-CASPT2// CASPT2	MS-CASPT2 + PCM// CASPT2 + PCM	URPA// UB3LYP[a]
$1^1A'$	0.00	0.00	0.00
$1^1A''$	2.20 (2.99 E − 06)	2.12 (1.69 E − 06)	3.18 (0.0002)
$2^1A'$	2.39 (3.65 E − 04)	2.32 (4.32 E − 04)	3.31 (0.3380)
$3^1A''$	4.00 (4.62 E − 01)	3.94 (5.09 E − 01)	3.48 (0.1919)
$1^3A'$	1.28	1.24	
$1^3A''$	2.16	2.07	
$2^3A'$	2.36	2.29	

[a]Ref. 17.

in Table 7, the predicted f value of $7A'$ is much larger than the others, which should be responsible for the experimentally observed absorption band ~360 nm (3.44 eV).[17] However, the calculated T_v values are about 0.50–0.60 eV larger than the experimental value. Similar problems were encountered before for CH_2I-I,[38] CH_2Br-I,[23] and CH_2I-Br.[23] Detailed theoretical calculation is undergoing for a reliable quantitative explanation.

PECs of the Spin-Free and Spin-Coupled States of CH_2Br_2

The ground state CH_2Br_2 was constrainedly optimized at different C—Br bond distances using the CASPT2 method, and the energies of the first five singlet and the first four triplet states were calculated at the corresponding optimized ground state geometries by the MS-CASPT2 method. Thus we obtained the PECs of CH_2Br_2 including nine spin-free states, see Figure 2a. As shown in Figure 2a, the photodissociation products of higher excited states (1^1A_2, 2^1A_1, and 1^3A_1) are not related with the ground-state products, i.e., the experimentally observed fast dissociation products ($CH_2Br\cdot + Br(^2P_{3/2})$ and $CH_2Br\cdot + Br^*(^2P_{1/2})$). So we do not need to consider these higher excited states for interpreting the photodissociation mechanism of CH_2Br_2. The MS-CASPT2//CASPT2 calculated T_v values of the first and second singlet excited states to be 5.64 and 5.80 eV, respectively, as listed in Table 4. Obviously, the experimentally employed 234 nm (5.30 eV),[21] 248 nm[19,22] and 267 nm[21] photon energy cannot reach 1^1B_1 and 1^1B_2 states vertically. The CASPT2 computed adiabatic excited energy (T_0) for 1^1B_1 and 1^1B_2 states of CH_2Br_2 is 4.90 and 4.91 eV, respectively. Therefore, the experimentally employed photon energy can make CH_2Br_2 transit from the ground state to the first two singlet excited states at most. As presented in Figure 2a, the PECs of the first two excited singlet and the first three triplet states are repulsive along the C—Br bond stretching coordinate and lead to the ground state products.

Figure 2a cannot give more information on the product of $Br^*(^2P_{1/2})$ or $Br(^2P_{3/2})$. Hence, the PECs of the corresponding seventeen spin-coupled states composed of the first five singlet and four triplet spin-free states in Table 4 were evaluated by the MS-CASPT2/CASSI-SO method. Those states higher than the fifteenth state have nothing to do with our concerns about the experimental observed photodissociation channels,[19,21,22] so we just included the PECs of the first fifteen states in Figure 2b. The spin-orbit-coupled PECs were drawn diabatically according to the composition of the spin-free states in the spin-coupled states. As clearly shown in Figure 2b, there are three groups of dissociation products as the C—Br bond stretches to the dissociation limit. The highest group originating from $3B_2$, $3B_1$, and $3A_2$ states (mainly composed of 1^3A_1) connects to very high excited states and is not related to the experimental observation. The energy difference between the lower two groups of dissociation products is 0.43 eV at R(C—Br) = 5.0 Å. This value agrees with the MS-CASPT2/CASSI-SO computed 0.43 eV[23] and the experimentally detected 0.46 eV[19,39] energy gap between $Br^*(^2P_{1/2})$ and $Br(^2P_{3/2})$. So, we assigned the ground group of

Table 7. The Calculated T_v (in eV) and f (in parentheses) Values and Characteristics of the Low-Lying Spin-Coupled States of CH_2Br-Br in the Gas and Solution Phases.

	MS-CASPT2/CASSI-SO//CASPT2			MS-CASPT2 + PCM/CASSI-SO//CASPT2 + PCM	
State	$T_v(f)$	Characteristic	State	$T_v(f)$	Characteristic
$1A'$	0.00	99.6% $1^1A'$	$1A'$	0.00	99.6% $1^1A'$
$1A''$	1.28 (0.00 E + 00)	97.9% $1^3A'$	$2A'$	1.29 (6.20 E − 06)	98.0% $1^3A'$
$2A'$	1.28 (1.22 E − 05)	97.8% $1^3A'$	$1A''$	1.29 (0.00 E + 00)	98.1% $1^3A'$
$2A''$	1.28 (3.05 E − 08)	98.0% $1^3A'$	$2A''$	1.29 (1.01 E − 08)	97.9% $1^3A'$
$3A'$	2.15 (3.86 E − 04)	79.2% $1^3A''$, 19.4% $2^3A'$	$3A'$	2.19 (4.26 E − 04)	79.0% $1^3A''$, 18.4% $2^3A'$
$3A''$	2.15 (0.00 E + 00)	76.8% $1^3A''$, 23.0% $2^3A'$	$3A''$	2.19 (0.00 E + 00)	76.4% $1^3A''$, 23.3% $2^3A'$
$4A'$	2.16 (2.46 E − 05)	79.7% $1^3A''$, 18.4% $2^1A'$	$4A'$	2.20 (5.28 E − 05)	78.2% $1^3A''$, 19.0% $2^1A'$
$4A''$	2.17 (2.12 E − 07)	74.1% $1^1A''$, 25.8% $2^3A'$	$4A''$	2.20 (6.38 E − 07)	75.1% $1^1A''$, 24.4% $2^3A'$
$5A'$	2.47 (4.31 E − 03)	70.8% $2^3A'$, 20.5% $1^3A''$, 7.9% $2^1A'$	$5A'$	2.51 (4.80 E − 03)	66.6% $2^3A'$, 20.7% $1^3A''$, 11.6% $2^1A'$
$5A''$	2.50 (1.50 E − 08)	75.9% $2^3A'$, 22.0% $1^3A''$	$5A''$	2.53 (2.07 E − 08)	75.9% $2^3A'$, 22.2% $1^1A''$
$6A''$	2.50 (3.00 E − 08)	73.3% $2^3A'$, 24.7% $1^1A''$	$6A''$	2.54 (3.87 E − 07)	74.5% $2^3A'$, 23.5% $1^1A''$
$6A'$	2.52 (5.60 E − 05)	71.4% $2^1A'$, 19.0% $1^3A''$, 8.0% $2^3A'$	$6A'$	2.55 (1.85 E − 04)	65.9% $2^1A'$, 20.7% $1^3A''$, 12.0% $2^3A'$
$7A'$	4.05 (6.17 E − 01)	99.5% $3^1A'$	$7A'$	3.95 (5.43 E − 01)	99.3% $3^1A'$

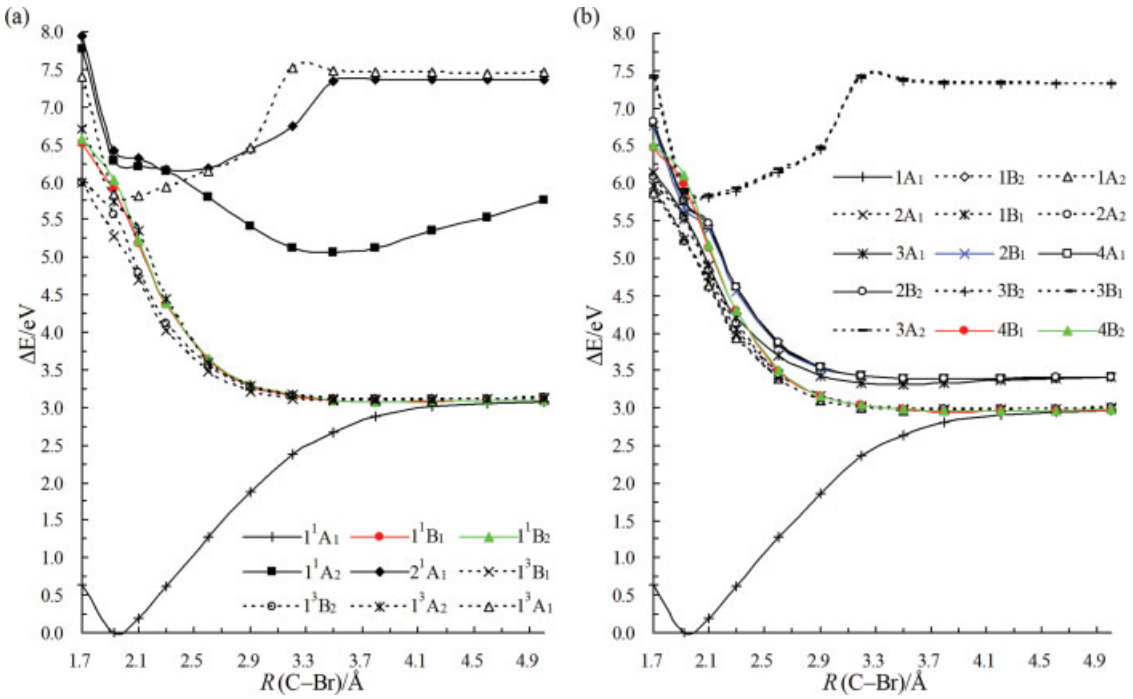

Figure 2. (a) The spin-free MS-CASPT2//CASPT2 PECs and (b) the spin-orbit-coupled MS-CASPT2/CASSI-SO//CASPT2 PECs, with respect to the C—Br bond coordinate of CH_2Br_2.

dissociation products to $CH_2Br\cdot$ + $Br(^2P_{3/2})$, and the upper group to $CH_2Br\cdot$ + $Br^*(^2P_{1/2})$. As shown in Figure 2b, products Br are originally from the $1B_2$, $1A_2$, $2A_1$, $1B_1$, $2A_2$, $4B_1$, and $4B_2$ states, while products Br* are from the $3A_1$, $2B_1$, $4A_1$, and $2B_2$ states. Many of these states have absolute zero or very small f values, which have no or very little contribution to the observed dissociation channels. Among them, the $2B_1$, $4B_1$, and $4B_2$ states are of f values larger than 1.0E-03. These three states should be important for assigning the experimentally observed dissociation channels. According to Table 5, most states have strong spin-orbit coupling. States $2B_1$ and $4B_1$ are of 9.6% and 77.5% composition of 1^1B_1, respectively. State $4B_2$ is mainly composed of the 1^1B_2 state. As presented in Figure 2b, state $2B_1$ directly dissociates to $CH_2Br\cdot$ + $Br^*(^2P_{1/2})$, while states $4B_1$ and $4B_2$ dissociate to $CH_2Br\cdot$ + $Br(^2P_{3/2})$. As shown in Table 5, states $4B_2$ and $2B_1$ have f values at the same level, which are much smaller than the f value of state $4B_1$. So, the photodissociation with Br recoil mostly occurs on the B_1 state, and the yield of Br is larger than that of Br*. This conclusion drawn from the present calculations agrees with the experimental observations.[17,19,21,22] The experiment[19] determined anisotropy parameter β value to be 1.0 ± 0.2, which indicates that the photodissociation with Br recoil mostly occurs on the B_1 state.

To consider solvent effects, the spin-free and spin-coupled states' PECs of CH_2Br_2 were also recalculated by the MS-CASPT2 + PCM and MS-CASPT2 + PCM/CASSI-SO methods, respectively. As shown in Figure S1 (see Supplementary Material Section), the PECs of CH_2Br_2 with consideration of solvent effects are very similar to the ones in the gas phase. Consequently, solvent effects do not affect the dissociation mechanism of CH_2Br_2.

Isomerization between CH_2Br_2 and CH_2Br—Br

Phillips and coworkers.[17] reported solvent effects on the A-band photodissociation of CH_2Br_2 by observing resonance Raman spectra in the solution phase. They considered that CH_2Br_2 may turn a photodissociation into a photoisomerization in the solution

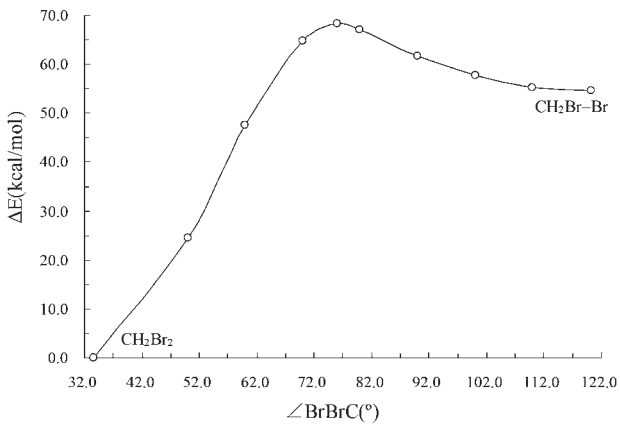

Figure 3. The CASPT2 + PCM//CASPT2 calculated PEC diagram depicting the isomerization between CH_2Br_2 and CH_2Br—Br in the solution phase.

phase. In the isomerization reaction, it is evident that the isomer $CH_2Br—Br$ is responsible for the ~360 nm transient absorption band observed upon ultraviolet photolysis of CH_2Br_2.[17] This absorption was assigned to the $7A'$ state of $CH_2Br—Br$ in section 3.3. This process cannot occur on the excited states, since the first several excited states are repulsive along the C—Br bond of CH_2Br_2 (see Fig. 2a). When the C—Br bond of CH_2Br_2 stretches to $CH_2Br\cdot$ + Br, the solvent cage effect induces the recombination of the $CH_2Br\cdot$ and Br fragments to $CH_2Br—Br$. We chose the bond angle ∠BrBrC as reaction coordinate and calculated the isomerization reaction path by the CASPT2 + PCM//CASPT2 method. As presented in Figure 3, the CASPT2 + PCM calculated activation energy from $CH_2Br—Br$ to CH_2Br_2 is 13.7 kcal/mol, and 68.3 kcal/mol for the inverse reaction. A transition state (TS) for the isomerization process was located by the CASPT2 full optimization (see Fig. 1 and Table 1) with only one imaginary frequency of 587 cm^{-1}.

Conclusions

The photodissociation of CH_2Br_2 in the gas and solution phases has been investigated by the MS-CASPT2/CASSI-SO and MS-CASPT2 + PCM/CASSI-SO methods, respectively. The calculated PECs of the spin-coupled states clearly assign the experimentally observed photodissociation channels leading to $CH_2Br\cdot$ + $Br(^2P_{3/2})$ and $CH_2Br\cdot$ + $Br^*(^2P_{1/2})$ in both gas and solution phases. For the photolysis of CH_2Br_2 in the solution, there is also an isomerization from CH_2Br_2 to $CH_2Br—Br$. But $CH_2Br—Br$ is much more unstable and prefers to turn back to CH_2Br_2.

References

1. Class, Th.; Ballschmiter, K. J Atmos Chem 1988, 6, 35.
2. Klick, S.; Abrahamsson, K. J Geophys Res 1992, 97, 12683.
3. Heumann, K. G. Anal Chim Acta 1993, 283, 230.
4. Mössigner, J. C.; Shallcross, D. E.; Cox, R. A. J Chem Soc Faraday Trans 1998, 94, 1391.
5. Friedrich, E. C.; Domek, J. M.; Pong, R. Y. J Org Chem 1985, 50, 4640.
6. Blomstrom, D. C.; Herbig, K.; Simmons, H. E. J Org Chem 1965, 30, 959.
7. Pienta, N. J.; Kropp, P. J. J Am Chem Soc 1978, 100, 655.
8. (a) Kropp, P. J.; Pienta, N. J.; Sawyer, J. A.; Polniaszek, R. P. Tetrahedron 1981, 37, 3229. (b) Kropp, P. J. Acc Chem Res 1984, 17, 131.
9. Causley, G. C.; Russell, B. R. J Chem Phys 1975, 62, 848.
10. Molina, L. T.; Molina, M. J.; Rowland, F. S. J Phys Chem 1982, 86, 2672.
11. Dixon, R. N.; Murrell, J. N.; Narayan, B. Mol Phys 1971, 20, 611.
12. Niessen, W. V.; Asbrink, L.; Bieri, G. J. Electron Spectrosc Relat Phenom 1982, 26, 173.
13. Tsai, B. P.; Baer, T.; Werner, A. S.; Lin, S. F. J Phys Chem 1975, 79, 570.
14. Ma, Z.-X.; Liao, C.-L.; Ng, C. Y. J Chem Phys 1993, 9, 6470.
15. Huang, J.; Xu, D.; Fink, W. H.; Jackson, W. M. J Chem Phys 2001, 115, 6012.
16. Chiang, S. Y.; Fang, Y. S.; Sankaran, K.; Lee, Y. P. J Chem Phys 2004, 120, 3270.
17. Zheng, X. M.; Kwok, W. M.; Phillips, D. L. J Phys Chem A 2000, 104, 10464.
18. Huang, J. H.; Xu, D. D.; Fink, W. H.; Jackson, W. M. J Chem Phys 2001, 115, 6012.
19. Lee, Y. R.; Chen, C. C.; Lin, S. M. J Chem Phys 2003, 118, 10494.
20. Sharma, P.; Vatsa, R. K.; Maity, D. K.; Kulshreshtha, S. K. Chem Phys Lett 2003, 382, 637.
21. (a) Tang, Y.; Ji, L.; Tang, B.-F.; Zhu, R.-S.; Zhang, S.; Zhang, B. Chem Phys Lett 2004, 392, 493. (b) Ji, L.; Tang, Y.; Zhu, R.-S.; Tang, B.-F.; Zhang, B. Chem Phys 2005, 314, 173. (c) Ji, L.; Tang, Y.; Zhu, R.-S.; Wei, Z.-R.; Zhang, B. Spectrochimica Acta Part A 2007, 67, 273.
22. Wei, P. Y.; Chang, Y. P.; Lee, W. B.; Hu, Z. F.; Huang, H. Y.; Lin, K. C.; Chen, K. T.; Chang, A. H. H. J Chem Phys 2006, 125, 133319.
23. Liu, Y.-J.; Ajitha, D.; Krogh, J. W.; Tarnovsky, A. N.; Lindh, R. Chem Phys Chem 2006, 7, 955.
24. (a) Andersson, K.; Malmqvist, P.-D.; Roos, B. O.; Sadlej, A. J.; Wolinski, K. J. Phys Chem 1990, 94, 5483. (b) Andersson, K.; Malmqvist, P.-D.; Roos, B. O. J Chem Phys 1992, 96, 1218.
25. Finley, J.; Malmqvist, P.-Å.; Roos, B. O.; Serrano-Andrés, L. Chem Phys Lett 1998, 288, 299.
26. Roos, B. O.; Malmqvist, P.-Å. Phys Chem Chem Phys 2004, 6, 2919.
27. Marian, C. M.; Wahlgren, U. Chem Phys Lett 1996, 251, 357.
28. Ghigo, G.; Roos, B. O. Chem Phys Lett 2004, 396, 142.
29. (a) Barone, V.; Cossi, M. J Phys Chem A 1998, 102, 1995. (b) Cossi, M.; Rega, N.; Scalmani, G.; Barone, V. J Chem Phys 2001, 114, 5691.
30. Roos, B. O.; Lindh, R.; Malmqvist, P.-Å.; Veryazov, V.; Widmark, P.-O. J Phys Chem A 2004, 108, 2851.
31. Karlström, G.; Lindh, R.; Malmqvist, P.-Å.; Roos, B. O.; Ryde, U.; Veryazov, V.; Widmark, P.-O.; Cossi, M.; Schimmelpfennig, B.; Neogrady, P.; Seijo, L. Comput Mater Sci 2003, 28, 222.
32. Kudchadker, S. A.; Kudchadker, A. P. J Phys Chem Ref Data 1975, 4, 457.
33. Davis, R. W.; Gerry, M. C. L. J Molec Spectrosc 1985, 109, 269.
34. Marshall, P.; Srinivas, G. N.; Schwartz, M. J Phys Chem A 2005, 109, 6371.
35. Maier, G.; Reisenauer, H. P.; Hu, J.; Schaad, L. J.; Jr; Hess, B. A. J Am Chem Soc 1990, 112, 5117.
36. (a) Bacher, W.; Wagner, J. Z. Phys Chem 1939, B43, 191. (b) Wagner, J. Z. Phys Chem 1939, B45, 69.
37. Maier, G.; Reisenauer, H. P. Angew Chem Int Ed Engl 1986, 25, 819.
38. Liu, Y.-J.; De Vico, L.; Lindh, R.; Fang, W.-H. Chem Phys Chem 2007, 8, 890.
39. Husain, D.; Donovan, R. J Adv Photochem 1971, 8, 1.